Appl. Phys. B 68, 419–423 (1999)

Applied Physics B
Lasers
and Optics

Invited paper

SHG studies of plasmon dephasing in nanoparticles

B. Lamprecht, A. Leitner, F.R. Aussenegg

Institut für Experimentalphysik der Karl-Franzens-Universität Graz and Erwin Schrödinger Institut für Nanostrukturforschung, Universitätsplatz 5, A-8010 Graz, Austria

Received: 14 October 1998/Revised version: 4 January 1999

Abstract. The decay time of the particle plasmon (dephasing of the coherent electron plasma oscillation) in Au and Ag nanoparticles is measured by a second-order nonlinear optical autocorrelation method in the fs regime. In order to prevent electron heating, the energy fluence from the fs pulses at the sample is kept below 0.5 $\mu J/cm^2$. The necessary high SHG efficiency is obtained by nanoparticles produced by an electron beam lithographic method, which enables us to fabricate a two-dimensional array of nearly identical, parallel oriented particles of designed shape without centrosymmetry, essential for high SHG efficiency and the tuning of the plasmon resonance to the driving laser wavelength of 780 nm.

PACS: 36.40.Gk; 78.47.+p; 61.46.+w; 71.45.Gm

Metal nanoparticles (MNPs) in transparent matrices are of high fundamental and practical interest, as they show spectrally selective optical absorption [1], can be used for surface enhanced Raman scattering [2] and are promising candidates for application as nonlinear optical media in all optical switching devices [3]. Further, metal nanostructures allow us to overcome the present miniaturization limits of light-guiding and light-handling optical devices, which has two practical consequences: the further miniaturization of opto-electronic systems in communications technology [4, 5], and the overcoming of present resolution limits in optical microscopy i.e. by optical near field microscopy [6]. Moreover, metal nanoparticles have shown several promising applications in optochemical sensorics, e.g. for enhancing the signals of optically monitored immunoreactions [7]. The whole field of nanoparticle and nanostructure optics represents a new subwavelength light technology and can be, in our opinion, expressed by the term "nanooptics".

In principle, all mentioned "applications" of metal nanoparticles and nanostructures are due to their ability to build up structural resonances of the collective oscillation of the metal's electron plasma, usually called localized surface plasmon or particle plasmon. Due to the confinement of the electrons in the metal structures (dielectric confinement), surface charges cause restoring forces when the plasma is driven by the incident light field and this leads to resonances.

Because of these resonances, MNPs are efficient and spectrally selective light absorbers and show the phenomenon of near field enhancement. The latter phenomenon occurs because the resonantly oscillating charges strongly enhance the electromagnetic field at and near the structures compared with the field strength of the irradiated light. Thus, metal nanostructures can concentrate light in matter with dimensions much smaller than the wavelength, a property for which various practical applications have already been found [3–7] and will surely be found in the future.

The central parameter for quantitative estimations in applications of MNPs is the resonance behavior of the plasma oscillation. In this article we focus on the damping properties of such resonances. The main damping mechanism of the collective, in-phase oscillation of the plasma electrons is caused by the electrical conductivity of the metal at light frequencies (optical conductivity). This value is given macroscopically by the imaginary part of the metal's dielectric function. In a simple Drude picture the conductivity is determined by the collision rate of the electrons with the lattice, which leads to a distribution in momentum. Thus, the amplitude of the coherent motion of the plasma electrons decays by a certain decay time T_2, which is a loss in coherence and may also be dedicated as "dephasing" in analogy to the dephasing time T_2 in molecular systems [8].

In a microscopic picture the decay time is determined by the coupling of the plasma oscillation to the electron–hole continuum where the dominating mechanism is bulk electron scattering [1]. The generated electron–hole pairs thermalize and increase the electron temperature. This may change the optical properties of the metal, measurable by ultrafast changes in reflectivity and transmissivity [9]. However, surface electron scattering from very small particles may also contribute significantly [1]. If the plasmon wavelength matches an interband transition of the metal, there is additional damping. Another damping mechanism is radiation damping, which increases with particle size and has to be taken into account above a size of approx. 50 nm [10].

As in any oscillator, the damping constant γ is represented by the homogenous line width $\Delta\nu_{\mathrm{hom}}$, which, however, is in practice not accessible by simple absorption or scattering spectroscopy of a particle ensemble, as it cannot be excluded that the measured line width contains additional inhomogenous contributions. As the resonance frequency of MNPs strongly depends on the particle shape [11], a distribution of this parameter causes such a contribution.

One way to overcome the problem of inhomogenous broadening due to a distribution in particle shapes is the spectroscopy of a single particle [12]. The other method to obtain $\Delta\nu_{\mathrm{hom}}$ and γ is the direct determination of the plasma oscillation's decay time τ_{pl}, for which $\tau_{\mathrm{pl}} = 1/(2\pi\,\Delta\nu_{\mathrm{hom}})$ is valid. From the experimentally obtained line width we can expect a decay time of a few femtoseconds.

In principle, all methods for measuring decay times use a two-pulse technique: the first pulse drives the system and the second, with variable time delay, probes the actual state. The method to be chosen for our purpose has to meet the following criteria, which excludes most of the conventional methods for decay time measurement: (i) Both measuring pulses must be irradiated collinearly onto the sample because any angle between them is accompanied by a geometrically induced timing error across the beam cross section in the fs regime [13, 14]. (ii) The photon flux within the beams must be kept below a certain limit in order not to change the electron temperature in the MNPs and therefore the optical constants, which would lead to an incorrect value of the decay time.

As a suitable method meeting the criteria given above, a second-order nonlinear optical autocorrelation method was found [14–16]. Figure 1 shows the well-known interferometric autocorrelation measurement set-up usually applied for femtosecond laser pulse characterization. The optical pulse is split into two pulses of identical power which are delayed with respect to each other by a variable mechanical delay before they are collinearly sent to an optically nonlinear crystal (BBO) for second-harmonic generation (SHG).

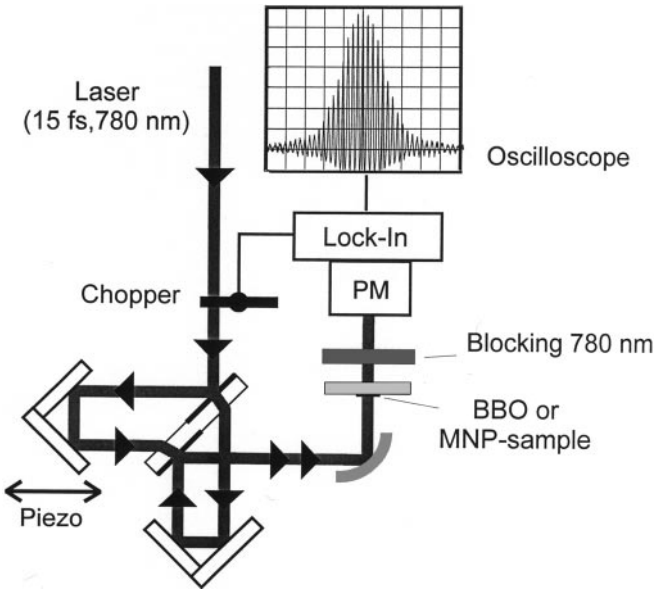

Fig. 1. Set-up for interferometric fs autocorrelation measurement. For measurement of the plasmon's field autocorrelation the BBO crystal is substituted by the MNP sample

The obtained function, SHG intensity versus delay time, is the pulse's second-order autocorrelation function (ACF) and contains the information on the pulse length. The identical set-up can also be used for determination of the autocorrelation function of the temporal development of the plasmon field in the MNPs by substituting the nonlinear crystal by the MNP sample. As the resonantly enhanced plasmon field drives a SH polarization in any metal surface [17], and consequently also in the surface of the MNP, the SH radiation produced is a precise monitor of the (squared) temporal behavior of the plasma oscillation. Thus the SH produced in the autocorrelation set-up represents the ACF of the plasmon's time function, which equals the correlation function of the two plasmons created by the two delayed laser pulses [14].

As the plasmon is a resonant system with a characteristic decay time, the resonant response to the laser pulse will be delayed and the oscillation will last longer than the laser pulse; see Fig. 2. The ACF of the squared plasmon response will consequently be broadened as shown in Fig. 6.

For application of this method the system under investigation must have a measurable optical nonlinearity originating directly from the process of interest, which in our case is the plasma oscillation. Under this assumption the system must follow the description of an anharmonic oscillator in the small-signal approximation. In that model the phenomenological second-order susceptibility $\chi^{(2)}(2\omega;\omega,\omega)$ is proportional to the squared linear susceptibility at the fundamental $\chi^{(1)}(\omega)$, and the linear susceptibility at the SH frequency $\chi^{(1)}(2\omega)$ [17, 18]:

$$\chi^{(2)}(2\omega;\omega,\omega) = -\frac{m\xi}{N^2e^3}\left[\chi^{(1)}(\omega)\right]^2\chi^{(1)}(2\omega) \qquad (1)$$

where m is the electron mass, N the plasma electron density, e the unit charge and ξ is a nonlinearity parameter. As the linear susceptibility $\chi^{(1)}$ has a maximum at the particle resonance frequency, it follows from (1) that the SH signal is strongly enhanced if the fundamental (or the SH frequency) equals the particle resonance (particle plasmon). Consequently, if the obtained frequency dependence of the SH efficiency follows the spectral dependence of the right-hand side of (1), this corroborates the assumption that the acting SH mechanism monitors the resonantly driven plasma oscillation at the fundamental and thus also the decay time extracted from the SH

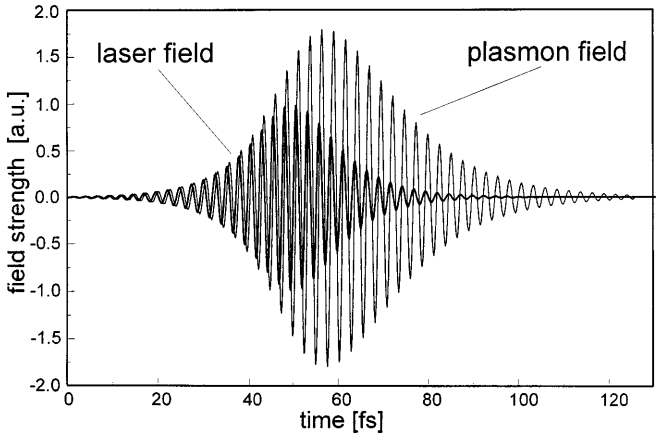

Fig. 2. Temporal behavior of the pulse laser field (*bold*) and the resonantly driven plasmon field (*thin*)

autocorrelation measurement represents the decaying plasma oscillation at the fundamental.

For the intended measurement of the decay time the metal particles have to meet several criteria which can hardly be met by particles fabricated by the simple technologies used, such as thermal evaporation, chemical deposition, etc. (a) The particles have to possess high SH efficiency at normal incidence of the fundamental. (b) In order to keep the photon flux low enough for electron gas heating to be neglected, for sufficient signal intensity, the SH efficiency must be as high as possible. (c) The particle resonance must be exactly at the fundamental.

These criteria were met by a method that allows tailoring of the particle shape and the arrangement pattern, thus the resonance frequency and the strength of particle interaction can be tuned independently. The chosen method is an advanced electron beam lithography technique (EBL) [19, 20]. EBL allows us to position metallic nanoparticles of any shape, size (down to a minimum curvature radius of approx. 20 nm) and orientation in any arrangement pattern on a flat (e.g. dielectric) substrate. The most important feature for this work is the possibility to design the symmetry properties of the individual particles in order to maximize the SHG efficiency when the incident fundamental beam is normal to the substrate plane.

For second-order optical nonlinearity the lack of centrosymmetry is a necessary condition. Although a metal particle's surface itself represents a noncentrosymmetric system, in a particle of rotational symmetric shape the integrated SH contributions of all surface elements destructively interfere and thus the SH efficiency at a fundamental incidence parallel to the rotation axis is zero in the dipole limit. Thus, MNPs of noncentrosymmetric shape must be used [21]. In order to design a particle with optimized SH efficiency at vertical incidence of the fundamental the following conditions have to be fulfilled: (i) The particle must have the greatest possible structural deviation from centrosymmetry. (ii) The particle must show plasmon resonance at the fundamental for a polarization direction that drives the strongest dipolar second-order nonlinear contribution.

Both criteria are well fulfilled by a composite particle (see Fig. 3). It is assembled from three identical coalescing particles each rotationally symmetric with the symmetry axis normal to the substrate plane. The particle centers are arranged at the edges of a right-angle triangle. The remaining symmetry elements characterize the particle of symmetry class $mm2$, which has five independent nonvanishing elements of the SHG tensor: xzx, yzy, zxx, zyy, zzz [22].

To drive the intended SHG tensor element (zzz) the particle should have the resonance at the fundamental for a polarization direction in the mirror symmetry plane (yz plane in Fig. 3) and at vertical incidence to the substrate plane (y direction). As the frequency tuning parameter, the height of the particle was used, which can easily be done by variation of the amount of deposited metal. Figure 4a,b shows the corresponding absorption spectra of such particles from gold in a quadratic arrangement pattern with a 480 nm grating constant for both polarization directions: (a) parallel (z axis in Fig. 3) and (b) perpendicular (x axis in Fig. 3) to the particle mirror plane. As can be seen in (a) the particle resonance could be tuned exactly to the laser wavelength at 780 nm by choosing the particle height as 23 nm. The spectrum shows two additional but weaker peaks which we assign to other modes of the system. For a polarization direction normal to the mirror plane (b) the spectrum is quite different, without a resonance at the fundamental. The width of the main peak is 75 nm and approximately equals the resulting homogenous line width. This shows that there is only a very small inhomogenous contribution due to a distribution in particle shapes, which was also proven by SEM measurements of the shape distribution.

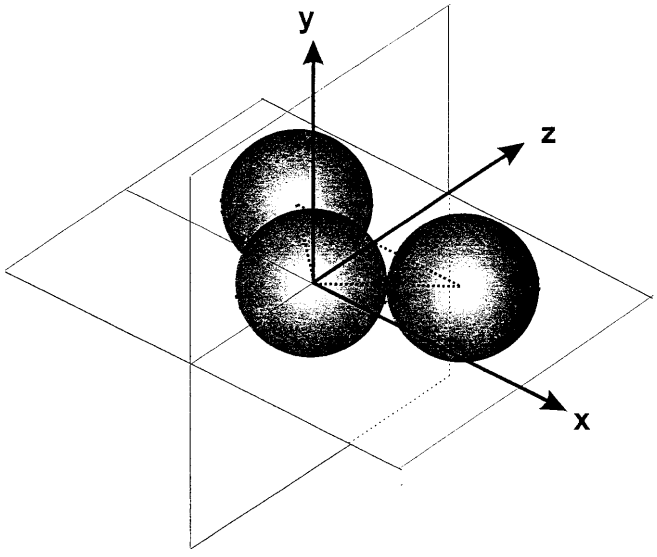

Fig. 3. Shape and coordinates of SHG optimized MNP

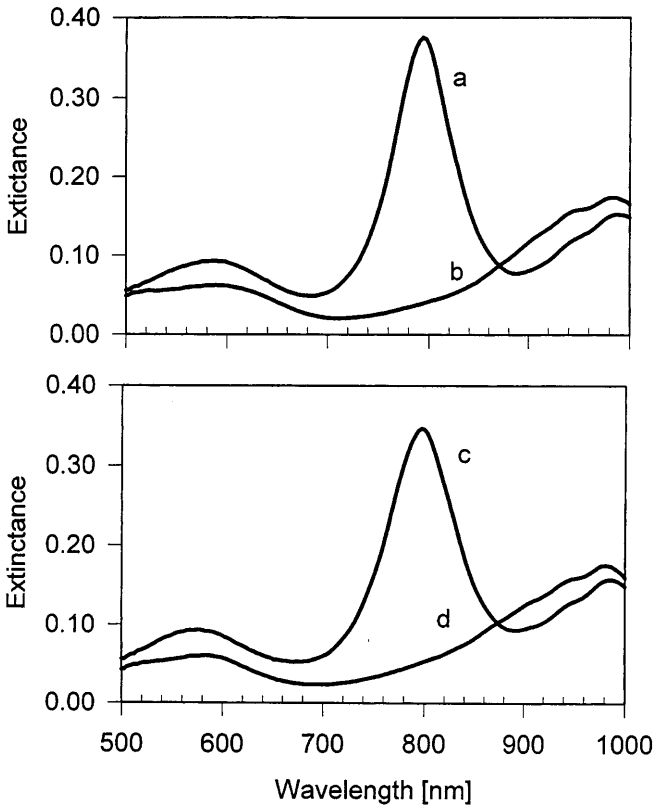

Fig. 4. Absorption spectra of the SHG optimized MNP shown in Fig. 3. for polarization direction parallel (a) and normal (b) to the mirror plane. (c), (d) are the corresponding spectra for identical particles but in a centrosymmetric arrangement pattern (see Fig. 5)

SHG efficiency measurements at particles with resonance frequencies differing from the fundamental laser wavelength show the expected dependence discussed above: the efficiency follows the wavelength dependence of the squared linear susceptibility $\chi^{(1)}(\omega)$ showing that the SHG really originates from the nonlinearity produced by the resonantly enhanced plasmon field.

In order to ensure that the strong SHG of the designed particles is mainly caused by the noncentrosymmetric shape of the particles, a reference system was designed as an array of identical particles in an identical arrangement pattern but with changed particle orientation so that the over-all symmetry of the system is now centrosymmetric. The SEM picture in Fig. 5 shows both cases, noncentrosymmetric (a) and centrosymmetric (b) particle arrangement. In Fig. 4c,d the linear absorption spectra of the centrosymmetric arrangement are shown for both polarization directions. As can be seen by comparison with Fig. 4a,b, the spectra are identical with the spectra of the noncentrosymmetric case. The SH efficiencies, however, at a fundamental wavelength of 780 nm with a polarization direction corresponding to case (a) in Fig. 5 are more than a factor 40 lower in the centrosymmetric case.

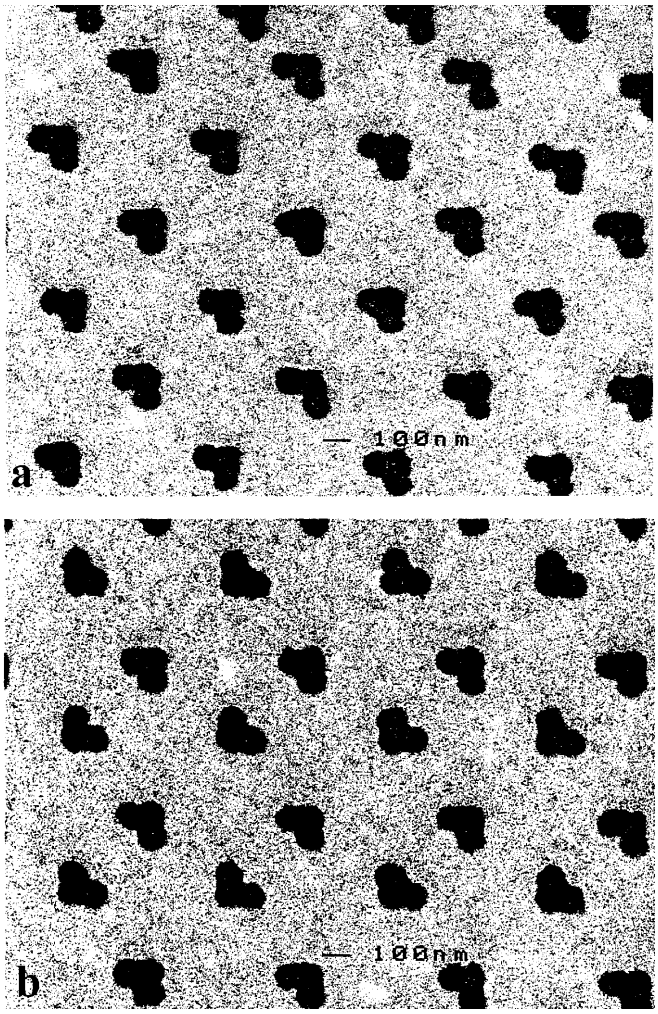

Fig. 5a,b. MNP arrangement pattern: non centrosymmetric (**a**) and centrosymmetric (**b**)

An autocorrelation measurement was performed with the noncentrosymmetric sample described above. Figure 6 shows the results for gold particles. The corresponding ACF of the laser pulse measured with a thin BBO crystal is shown by the bold line. As can be clearly seen, the ACF of the particles is broader than the ACF of the exciting laser pulse. The evaluation of the measured ACF is done by comparison with a model ACF. In the simulation, a distribution of harmonic oscillators with variable decay time (damping) was driven by the field of a sech^2-shaped 15-fs laser pulse corresponding to the experimentally used laser pulse characterized by the BBO measurement (Kerr-lens mode-locked Ti:sapphire laser; group velocity dispersion compensated by chirped mirrors, central wavelength of 780 nm). The accuracy of this method is ± 1 fs. This evaluation method is used to obtain the plasmon decay time from the measured ACF even in the case of an inhomogenously broadened absorption due to unequally shaped particles in the sample array [23]. The pulse energy fluence at the sample was kept below $0.5\,\mu\mathrm{J/cm}^2$ where no dependence of the decay time on the intensity was observed, which ensures that changes in the nonlinear optical efficiency caused by electron heating [9] can be neglected.

The resulting plasmon decay times τ_{pl} for Ag and Au particles of the described noncentrosymmetric shape and arrangement pattern (Fig. 5a), deposited on an indium-tin-oxide-coated (ITO) glass substrate (ITO thickness of 30 nm) [14] are shown in Table 1 and compared with the decay time deduced from ε'' values of the bulk metal at $\lambda =$

Table 1. Measured and calculated plasmon decay times for Au and Ag at $\lambda = 780$ nm

	τ_{pl}/fs measured	τ_{pl}/fs calculated
Au	6 ± 1	7 ± 1
Ag	$7 \div 10$	$12 \div 37$

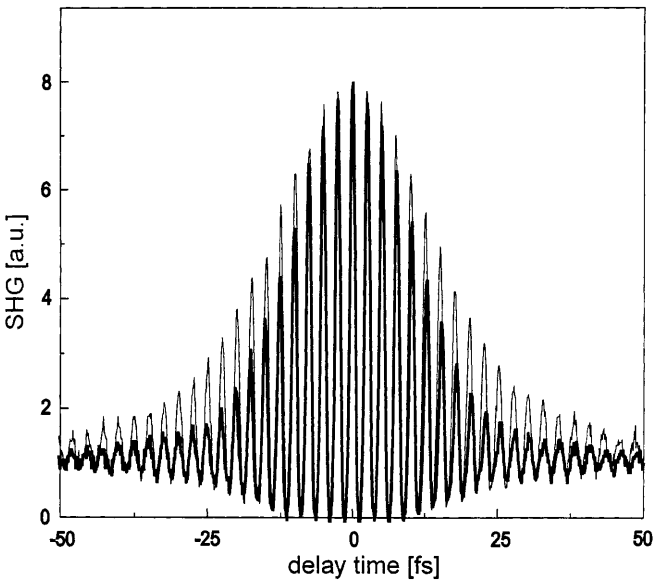

Fig. 6. Interferometric autocorrelation functions for the laser pulse (*bold*) measured with BBO crystal and the MNP's plasmon (*thin line*) for gold as the metal

780 nm (exciting wavelength) by a single-particle model [11] with radiation damping taken into consideration.

For gold the experimentally obtained and modeled values agree very well. In the case of silver the experimentally obtained values vary between 7 and 10 fs, depending on preparation conditions such as substrate roughness, lithographic processing parameters, etc. This finding and the fact that calculated decay times found by using bulk values are longer than those found experimentally in any case, suggests that in the case of silver, in contrast to gold, surface chemical damping mechanisms are active [1, 24]. Due to the different bulk values of the silver dielectric function listed in the literature [25, 26] the calculated decay times for silver vary considerably depending on the data source used.

For gold particles, single-particle spectroscopy was used to give a value of 8 fs for the dephasing time of the polarization T_2 [12]. As this dephasing time is related to the plasmon decay time by $T_2 = 2\tau_{\mathrm{pl}}$ the comparable value of these measurements is 4 fs. Taking into account that these measurements have been performed at a wavelength of 630 nm where interband transitions cause stronger absorptions than at 780 nm this result agrees very well with ours.

Acknowledgements. Finally support by the Austrian Federal Ministry for Science and Traffic, Technology Division, is grateful acknowledged.

References

1. U. Kreibig, M. Vollmer: *Optical Properties of Metal Clusters* (Springer, Berlin, Heidelberg 1995)
2. R.K. Chang, T.E. Furtak: *Surface enhanced Raman scattering* (Plenum, New York 1981)
3. R.F. Haglund, Jr., L. Yang, R.H. Magruder III, J.E. Wittig, K. Becker, R.A. Zuhr: Opt. Lett. **18**, 373 (1992)
4. J. Takahara, S. Yamagishi, H. Taki, A. Morimoto, T. Kobayashi: Opt. Lett. **22**, 475 (1997)
5. M. Quinten, A. Leitner, J.R. Krenn, F.R. Aussenegg: Opt. Lett. **23**, (1998)
6. O. Marti, R. Möller (Eds.): *Photons and local probes*, NATO ASI Series, Ser. E: Appl. Sci. **300** (Kluwer, Dordrecht 1994)
7. T. Schalkhammer: Chem. Monthly **129**, 1067 (1998)
8. F.J. Heilweil, R.M. Hochstrasser, J. Chem. Phys. **82**, 4762 (1985)
9. J. Hohlfeld, J.G. Müller, S.-S. Wellershoff, E. Matthias: Appl. Phys. B **64**, 387 (1996)
10. A. Wokaun, J.P. Gordon, P.F. Liao: Phys. Rev. Lett. **48**, 957 (1982)
11. C.F. Bohren, D.R. Huffman: *Absorption and Scattering of Light by Small Metal Particles* (Wiley, New York 1983)
12. T. Klar, M. Perner, S. Grosse, G. von Plessen, W. Spirkl, J. Feldmann: Phys. Rev. Lett. **80**, 4249 (1998)
13. A.A. Maznev, T.F. Crommins, K.A. Nelson: Opt. Lett. **23**, 1378 (1998)
14. B. Lamprecht, A. Leitner, F.R. Aussenegg: Appl. Phys. B **64**, 269 (1997)
15. J.H. Klein-Wiehle, P. Simon, H.G. Rubahn: Phys. Rev. Lett. **80**, 45 (1998)
16. A. Assion, B. Lang, M. Simon, S. Voll, F. Träger, G. Gerber: SPIE Proc. **3273**, 15 (1998)
17. R. Shen: *The Principles of Nonlinear Optics* (Wiley, New York 1984)
18. F. Zernicke, J.E. Midwinter: *Applied Nonlinear Optics* (Wiley, New York 1973)
19. W. Gotschy, K. Vonmetz, A. Leitner, F.R. Aussenegg: Opt. Lett. **21**, 1099 (1996)
20. W. Gotschy, K. Vonmetz, A. Leitner, F.R. Aussenegg: Appl. Phys. B **63**, 381 (1996)
21. F.R. Aussenegg, A. Leitner, H. Gold: Appl. Phys. A **60**, 97 (1995)
22. N. Bloembergen, Y.R. Shen: Phys. Rev. **141**, 141 (1965)
23. B. Lamprecht, A. Leitner, F.R. Aussenegg: submitted to Appl. Phys. B
24. B.N.J. Persson: Surf. Sci. **281**, 153 (1993)
25. P.B. Johnson, R.W. Christy: Phys. Rev. B **6**, 4370 (1971)
26. E.D. Palik (Ed.): *Handbook of Optical Constants of Solids* (Academic Press, Boston, MA 1985)